



Photoluminescence emissions of $\text{Ca}_{1-x}\text{WO}_4:x\text{Eu}^{3+}$: Bridging between experiment and DFT calculations[☆]

Amanda Fernandes Gouveia^{a, b, *}, Marcelo Assis^{a, c}, Lara Kelly Ribeiro^c,
Aline Estefany Brandão Lima^d, Eduardo de Oliveira Gomes^b, Daniele Souza^e,
Yara Gobato Galvão^e, Ieda Lucia Viana Rosa^c, Geraldo Eduardo da Luz Jr.^d,
Eva Guillamón^a, Elson Longo^c, Juan Andrés^{a, **}, Miguel Angel San-Miguel^b

^a Department of Physical and Analytical Chemistry, University Jaume I (UJI), 12071, Castelló, Spain

^b Institute of Chemistry, State University of Campinas (Unicamp), 13083-970, Campinas, SP, Brazil

^c CDMF, Federal University of São Carlos (UFSCar), P.O. Box 676, 13565-905, São Carlos, São Paulo, Brazil

^d Departamento de Química, Federal University of Piauí (UFPI), 64049-550, Teresina, Piauí, Brazil

^e Physics Department, Federal University of São Carlos (UFSCar), P.O. Box 676, 13565-905, São Carlos, São Paulo, Brazil

ARTICLE INFO

Article history:

Received 28 May 2021

Received in revised form

9 August 2021

Accepted 30 August 2021

Available online 15 October 2021

Keywords:

$\text{Ca}_{1-x}\text{WO}_4:x\text{Eu}^{3+}$

DFT calculations

Photoluminescence emissions

Rare earths

ABSTRACT

In this work, the impact of the doping process on the photoluminescence emission of CaWO_4 as a function of the concentration of Eu^{3+} cation (0.01 mol%, 0.02 mol%, 0.04 mol%, 0.06 mol%, 0.08 mol%, and 0.10 mol%) is discussed in detail. $\text{Ca}_{1-x}\text{WO}_4:x\text{Eu}^{3+}$ samples were successfully synthesized by a simple co-precipitation method followed by microwave irradiation. The blue shift in the absorption edge confirms the quantum confinement effect and the band gap energy covers the range from 3.91 to 4.18 eV, as the amount of Eu^{3+} cations increases. The experimental results are sustained by first-principles calculations, at the density functional theory level, to decipher the geometry and electronic properties, thereby enabling a more accurate and direct comparison between theory and experiment for the $\text{Ca}_{1-x}\text{WO}_4:x\text{Eu}^{3+}$ structure.

© 2021 The Authors. Published by Elsevier B.V. on behalf of Chinese Society of Rare Earths. This is an open access article under the CC BY-NC-ND license (<http://creativecommons.org/licenses/by-nc-nd/4.0/>).

1. Introduction

The high chemical stability of CaWO_4 (CW)-based phosphors and the excellent photoluminescence (PL) emissions have attracted a lot of attention due to their ability of serving as a luminescence host with low phonon threshold energy and wide visible emission spectra.^{1–6}

Lanthanide luminescence has become essential in the lighting industry,⁷ and the Eu^{3+} cations are the most studied activators in

the rare-earth cations (RE^{3+}) family with intense emissions located in the visible region, displaying higher luminescence purity and quantum yields.^{8–13} The substitution of Ca^{2+} by Eu^{3+} cations leads to the formation of $[\text{EuO}_8]$ clusters. $\text{Ca}_{1-x}\text{WO}_4:x\text{Eu}^{3+}$ (CWE) doped materials have been obtained through different synthesis methods. Zhang et al. analyzed the effect of synthesis conditions, such as pH, temperature, and doping concentrations, on the morphology and sizes of CWE.¹⁴ Xiong et al. prepared CWE nanoparticles with excellent load-carrying capacity, wear resistance, and friction-reducing properties in a water-soluble fluid.¹⁵ Very recently, the precipitation route to obtain CW nanoparticles containing Eu^{3+} and Dy^{3+} cations was used by Kaur et al.¹⁶

The changes induced by the addition of Eu^{3+} cations in different concentrations in the CW host matrix enhance their performance, because this material has numerous scientific and technological applications, such as light-emitting diodes converted into phosphors, sensors, capacitors, catalysts, etc.^{15,17–19} In particular, the CWE samples were previously obtained with different

[☆] **Foundation item:** Project supported in part by Fundação de Amparo à Pesquisa do Estado de São Paulo - FAPESP (2013/07296-2; 2016/23891-6; 2017/26105-4; 2019/01732-1), Financiadora de Estudos e Projetos - FINEP, Conselho Nacional de Desenvolvimento Científico e Tecnológico - CNPQ (166281/2017-4, 305792/2020-2), and CAPES.

* Corresponding author. Department of Physical and Analytical Chemistry, University Jaume I (UJI), 12071, Castelló, Spain.

** Corresponding author.

E-mail addresses: gouveiad@uji.es (A.F. Gouveia), andres@qfa.uji.es (J. Andrés).

concentrations of Eu^{3+} cation and the PL properties as well as the chromaticity coordinates and lifetimes of the samples were investigated.²⁰

This paper reports a combined experimental and theoretical work to investigate the events that occur in the PL activity and their relationship with the excited electronic states of Eu-doped CW crystals. The main novelty of this study is the use of first-principles quantum-mechanical calculations, at the density functional theory (DFT) level, to study and predict the structure and PL emissions, which would promote the development of CWE based phosphors. The samples were prepared by a simple co-precipitation (CP) method followed by microwave irradiation (MI) without any surfactant. This enabled to be promising materials in inorganic single-emitting component regions for optical applications.

2. Experimental and theoretical procedure

2.1. Synthesis and characterizations

The synthesis of CW sample was performed using the CP method followed by MI. 1×10^{-3} mol of $\text{Ca}(\text{CH}_3\text{CO}_2)_2 \cdot \text{H}_2\text{O}$ (Aldrich, 99%) and 1×10^{-3} mol of $\text{Na}_2\text{WO}_4 \cdot 2\text{H}_2\text{O}$ (Aldrich, 99%) were added in two separate beakers containing 50.0 mL of distilled water each. The $\text{Ca}(\text{CH}_3\text{CO}_2)_2 \cdot \text{H}_2\text{O}$ solution was then added to the $\text{Na}_2\text{WO}_4 \cdot 2\text{H}_2\text{O}$ solution, and the suspension was transferred to a Teflon autoclave, sealed, and placed in the microwave assisted hydrothermal system (2.45 GHz, maximum power of 800 W). The reaction mixture was heated to 160 °C for 32 min. The products were washed with deionized water several times and dried at 60 °C for 12 h.

For the CWE samples, the same procedure described above was done with the addition of 0.01 mol%, 0.02 mol%, 0.04 mol%, 0.06 mol%, 0.08 mol%, and 0.10 mol% of Eu^{3+} and the removal of the corresponding Ca^{2+} mass. The reagent used was $\text{Eu}(\text{NO}_3)_3$ which was obtained from dissolution of Eu_2O_3 (Aldrich, 99.9%) in HNO_3 , followed by the neutralization and dilution with water. The doped samples were called as CWE1, CWE2, CWE4, CWE6, CWE8, and CWE10 for 0.01 mol%, 0.02 mol%, 0.04 mol%, 0.06 mol%, 0.08 mol%, and 0.10 mol% Eu^{3+} , respectively.

The CW and CWE samples were structurally characterized by different techniques such as: X-ray diffraction (XRD) with Rietveld refinement analysis, field emission scanning microscopy (FE-SEM), spectroscopies of micro-Raman (MR) and Fourier transform infrared (FT-IR), ultraviolet-visible (UV-Vis) absorption, energy dispersive (EDS), X-ray photoelectron (XPS), and X-ray fluorescence (XRF).

The XRD using a D/Max-2500PC diffractometer (Rigaku, Japan) with $\text{Cu K}\alpha$ radiation ($\lambda = 0.15406$ nm) in the 2θ range of 10° – 110° with a scanning speed of 1 ($^\circ$)/min. FE-SEM and EDS were performed using an equipment Inspect F50 (FEI Company, Hillsboro, OR), operated at 15 kV. UV-vis diffuse reflectance measurements were obtained using a Cary 5G spectrophotometer (Varian, USA) in diffuse reflection mode. The MR spectra were obtained by the Micro Raman spectrometer (HORIABA Jobin Yvon T64000) with a radiation of 514 nm in the 50 – 3500 cm^{-1} range. The FT-IR was performed using a Jasco FT/IR-6200 (Japan) spectrophotometer operated in turn mode at room temperature and the spectra were carried out in the range of 470 – 4000 cm^{-1} . A Kimmon He-Cd laser (325 nm laser; 40 mW maximum power) was used as the excitation source for PL measurements. XPS analyses were performed on a Scientia Omicron ESCA spectrometer (Germany) using a monochromatic X-ray source of Al $\text{K}\alpha$ (1486.7 eV). Peak deconvolution was performed using a 70%:30% Gaussian-Lorentzian line shape and a Shirley nonlinear sigmoid-type baseline. The binding energies of all elements were calibrated with reference to the C 1s

peak at 284.8 eV. Element analysis of the samples was performed with an XRF 720 (Shimadzu Corp, Kyoto, Japan) operating at 4 kV and 80 mA. The luminescence lifetime measurements were carried out as well using a 1940D model spectrophotometer coupled to the spectrofluorometer.

2.2. Computational methods

First-principles calculations were performed to study the effect of Eu doping on the CaWO_4 structure. In this way, two models were constructed, the pure CW and CWE. All calculations were performed with the CRYSTAL17 software package.^{21,22} The CRYSTAL package performed *ab initio* calculations of the ground state energy, energy gradient, electronic wave function and properties of periodic systems. Hartree-Fock or KohnSham Hamiltonians (that adopted an Exchange-Correlation potential following the postulates of Density-Functional Theory) can be used. Periodic systems in 0 (molecules, 0D), 1 (polymers, 1D), 2 (slabs, 2D), and 3 dimensions (crystals, 3D) are treated on an equal footing. In each case the fundamental approximation made is the expansion of the single particle wave functions ("Crystalline Orbital", CO) as a linear combination of Bloch functions (BF) defined in terms of local functions (hereafter indicated as "Atomic Orbitals", AOs).

The computational method is based on the DFT associated with B3LYP hybrid functional.^{23,24} Ca, W, O, and Eu atomic centers were described by the Ag_HAYWSC-311d31G_apra_1991, W_cora_1996, and O_6-31d1_corno_2006 basis sets, respectively, which were obtained from the Crystal website.^{25,26} The diagonalization of the Fock matrix was performed using a $6 \times 6 \times 6$ grid with 44k-point grids in the reciprocal space. The thresholds controlling the accuracy of the calculation of the Coulomb and exchange integrals were set to 10^{-8} , 10^{-8} , 10^{-8} , 10^{-8} , and 10^{-16} , and the percentage of Fock/Kohn-Sham matrix mixing was set to 30.

A full optimization process of the lattice parameters (a and c) and the internal atomic coordinates (x , y , and z) for the bulk was carried out until all force components were less than 10^{-5} eV/nm.² From this optimized bulk structure, two periodic models, were built by selecting a $2 \times 2 \times 2$ supercell: (1) the pure CW model of 192 atoms in the structure, composed by 32 Ca atoms, 32 W atoms and 128 O atoms and (2) the CWE model, in which two Ca^{2+} cations were replaced by two Eu^{3+} cations. To keep the electroneutrality of the system, a Ca^{2+} cation ghost was considered. This model contains 6.90% molar Eu in the structure. The band structure and density of states (DOS) of the CW and CWE models were obtained for 200 \vec{k} points along the appropriate high-symmetry directions of the corresponding irreducible Brillouin zone.

3. Results and discussion

An analysis of the XRD patterns of the CW and CWE samples in Fig. 1 renders that all materials exhibit well defined diffraction peaks, corresponding to the scheelite phase with tetragonal structure and space group $I4_1a$; this was in accordance with card No. 5510²⁷ in the Inorganic Crystal Structure Database (ICSD). There was no secondary phase formation, indicating that the Eu^{3+} cation substitution process takes places successfully.

From the structural point of view, the lattice of the CW is composed by distorted octahedra $[\text{CaO}_8]$ and tetrahedra $[\text{WO}_4]$ clusters, in which the Ca atoms are coordinated with eight O atoms in an octahedral symmetry, while the W atoms are surrounded by four O atoms (see Fig. 2); each $[\text{CaO}_8]$ cluster shares corners with eight $[\text{WO}_4]$ tetrahedra to form chains parallel to $[110]$ direction.

Assuming that the samples present a spherical morphology, the average crystallite size (D) and the lattice strain (ϵ) of the as-

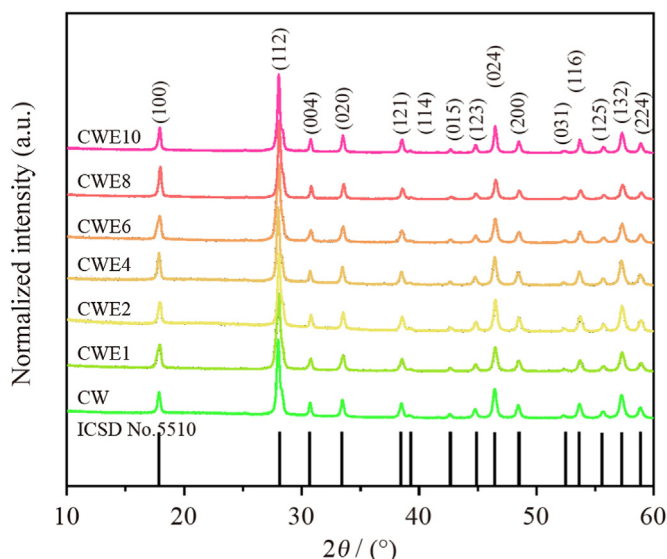


Fig. 1. XRD patterns of the CW and CWE samples.

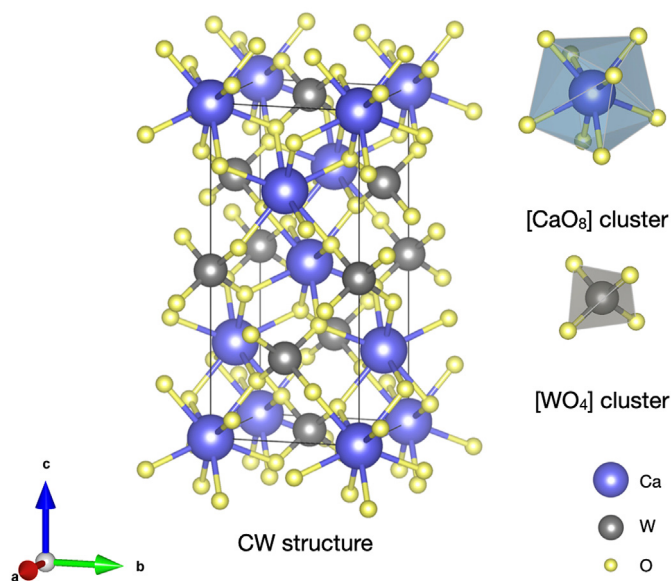


Fig. 2. CW structure and the distorted octahedra $[\text{CaO}_8]$ and tetrahedra $[\text{WO}_4]$ clusters. The substitution of the Ca^{2+} by Eu^{3+} cation leads to the formation of $[\text{EuO}_8]$ clusters.

synthesized samples were calculated and the values are presented in Table 1. The D value was obtained through the Scherrer's equation (Eqs. (1)–(2)), using the full width half maximum (FWHM) of the most intense peak [112].

Table 1
FWHM ($^\circ$) values, crystallite size and lattice strain calculated from XRD data.

Sample	FWHM ($^\circ$)	D (nm)	ϵ (10^{-3})
CW	0.297	28.819	10.249
CWE1	0.276	31.018	6.030
CWE2	0.293	29.217	7.510
CWE4	0.299	28.626	10.318
CWE6	0.395	21.672	10.124
CWE8	0.294	29.116	8.279
CWE10	0.287	29.829	6.270

$$D = \frac{0.89\lambda}{\beta \cos\theta} \quad (1)$$

$$\beta = \sqrt{\beta_e^2 - \beta_s^2} \quad (2)$$

where D is the average crystallite size, λ the X-ray wavelength (0.15406 nm), θ the Bragg angle, β_e the experimental full width at half maximum (FWHM) of the sample and β_s the FWHM of LaB_6 standard.²⁸ The ϵ parameter²⁹ can be obtained by Eq. (3):

$$LS = \frac{\beta}{4 \tan\theta} \quad (3)$$

An elemental analysis of the CWE samples was performed by XRF spectrometry to obtain effective amount of Eu^{3+} cations along the doping process at the CW lattice and the results are in Table 2. The X-ray energy (spectral line $L\alpha$) for the Eu element was observed to be 5.849 keV. The amount of Eu^{3+} cations obtained by XRF compared to the nominal concentration of each sample is very close, confirming the substitution of Ca^{2+} by Eu^{3+} cations in the CW lattice.

The distribution of Ca, W, O and Eu atoms in the CWE10 sample was analyzed by EDS mapping and a homogeneous distribution for all elements in the micro-dumbbells morphology was observed, as can be seen in Fig. SI-1 (see the Supporting Information, SI).

The XPS technique was used as a powerful tool to qualitatively determine the surface composition of the materials. According to the results (see Fig. SI-2), the characteristic peaks of Ca, W and O display that the samples are of high purity and the doping process of Eu^{3+} cations takes place at the sites occupied by the Ca^{2+} cations. This analysis also demonstrated that the Eu content in the region close to the surface is much lower than that of the bulk. More details can be found in the XPS section in the SI.

Fig. 3(a) shows the MR spectrum in the range of 50–3500 cm^{-1} . Two different regions can be sensed, one related to CaWO_4 (Fig. 3(b)) and the other related to Eu substitution (Fig. 3(c)) since such modes are observed only with substitution. Both parts of the spectrum presented well defined modes, showing a high degree of order of the samples at short-range. Fig. 3(b) shows the spectrum of 50–1000 cm^{-1} which is related to CW and a full discussion of these modes can be found in the SI. In the spectrum of Fig. 3(c), the bands at 2536.3, 2957.1, 3112.0, and 3195.7 cm^{-1} can be sensed. These bands become even more intense as the amount of Eu^{3+} cations increases and, according to Tiseanu et al., these bands correspond to a fingerprint of substitution by Eu^{3+} cations in a tetragonal structure.³⁰ The analyses of the FT-IR spectra were also performed, and the discussion can be found in the SI.

For the study of the optical behavior of CWE samples, it was performed by calculating the band gap energy (E_{gap}) using the method proposed by Kubelka and Munk (more details in SI). Fig. SI-4 shows that the band gap structures of the CW and CWE samples are characteristic of well-defined direct transitions, which is of the

Table 2
Amount of Eu^{3+} cations obtained by XRF spectrometry and the nominal values.

Sample	Experimental	Nominal
CW	0.0000	0.0000
CWE1	0.0112	0.0100
CWE2	0.0181	0.0200
CWE4	0.0409	0.0400
CWE6	0.0571	0.0600
CWE8	0.0816	0.0800
CW10	0.0972	0.1000

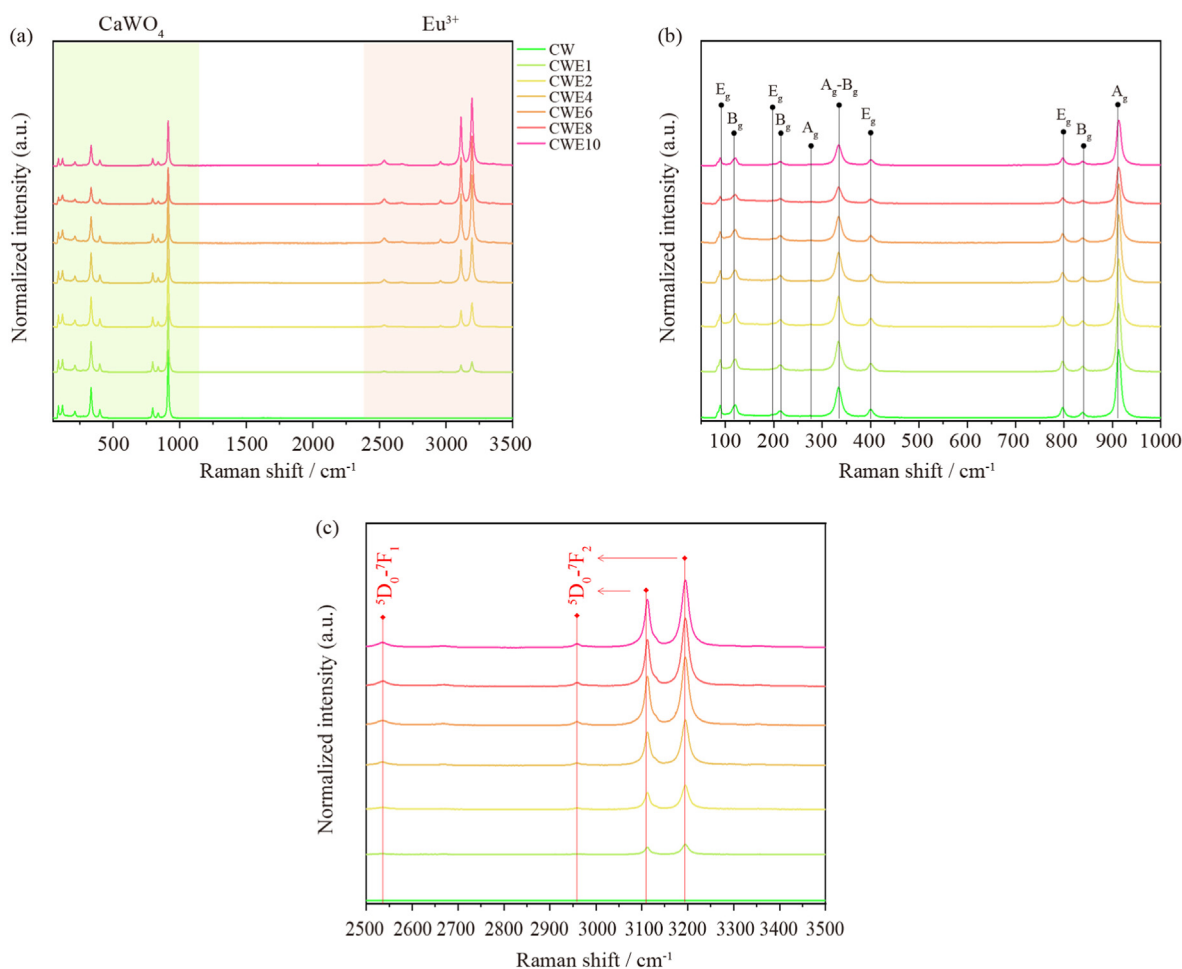


Fig. 3. (a) Micro Raman spectra of CW and CWE samples; (b) Zoom of the region between 50 and 1000 cm^{-1} ; (c) Zoom of the region between 2500 and 3500 cm^{-1} .

nature of crystalline semiconductors. The CW sample presented an E_{gap} of 4.12 eV, the CWE samples presented E_{gap} of 3.91, 4.01, 4.11, 4.09, 4.10, and 4.18 eV, respectively in ascending order of doping Eu^{3+} cations. The decreasing in the E_{gap} can be attributed to the existence of structural defects localized in the forbidden band gap region.

By using the results of the DFT calculations an analysis of the energy levels in the valence band (VB) and the conduction band (CB) was performed (see Fig. 4(a, b)). As can be seen, a direct electronic transition at the Γ -point in the Brillouin zone can be sensed. The CWE model has a lower band gap value (3.90 eV) when compared with the CW model (5.71 eV). This decrease of the band gap is due to the structural defect caused by the substitution of Ca^{2+} by Eu^{3+} cations, which involves the creation of new energy levels between the VB and CB.

In Fig. 4(c, d), the DOS for the CW and CWE models are displayed, respectively. An analysis of the results renders that despite the small contribution to CB from the Eu orbitals, the presence of Eu^{3+} cations in the CW structure caused a perturbation in the electronic states into the two bands (VB and CB). The position of Fermi level changed, from -4.40 eV in the CW model to -3.36 eV in the CWE model, while the first empty level in CB, goes from 1.31 to 0.44 eV. In both theoretical models, VB is formed mainly by the 2p orbitals of the O atoms, while CB is composed mainly by the hybridization of the 5d and 2p orbitals, between W and O atoms, respectively.

In order to analyze the morphology of the samples in function of the Eu^{3+} cations concentration, the FE-SEM was performed and images of CW and CWE samples are shown in Fig. 5. For the CW sample, the formation of microspheres and micro-dumbbells is observed, with an average size of $4.05 \pm 0.49 \mu\text{m}$ (Fig. 5(a)). The microspheres have already been obtained by conventional hydrothermal,^{31,32} sonochemical³³ and reverse micelle methods³⁴; while the micro-dumbbells morphology was obtained by the microwave hydrothermal method.³⁵ For the CWE samples (Fig. 5(b-g)), the formation of microspheres was not observed, obtaining only micro-dumbbells with sizes of 4.22 ± 0.45 , 4.27 ± 0.57 , 4.24 ± 0.42 , 4.29 ± 0.43 , 4.91 ± 0.88 , $4.95 \pm 0.57 \mu\text{m}$ for samples CWE1, CWE2, CWE4, CWE6, CWE8, and CWE10, respectively.

The PL emissions of the samples with different amounts of Eu^{3+} cations are displayed in Fig. 6(a). The pure CW has a broadband emission profile, characteristic of a multiphonic process, involving several intermediate energy states. The maximum emission of the CW sample is found at, approximately, 500 nm, in the cyan-green region, which are the result of internal charge transfers from the $[\text{WO}_4]$ clusters and oxygen vacancy (V_O) in the $[\text{WO}_4]$ and $[\text{CaO}_8]$ clusters.^{4,36} With the replacement of Ca^{2+} by Eu^{3+} cations, the appearance of specific transitions of Eu^{3+} is observed ($^5\text{D}_0 \rightarrow ^7\text{F}_j$, $j = 1, 2, 3$, and 4), with maximum emission located at 596, 616, 659, and 704 nm, and these become more intense with the increased concentration of Eu^{3+} cations (Fig. 6(a)).³⁷ The intensities of the observed transitions are dependent on the coordination of the Eu^{3+} cations.³⁸

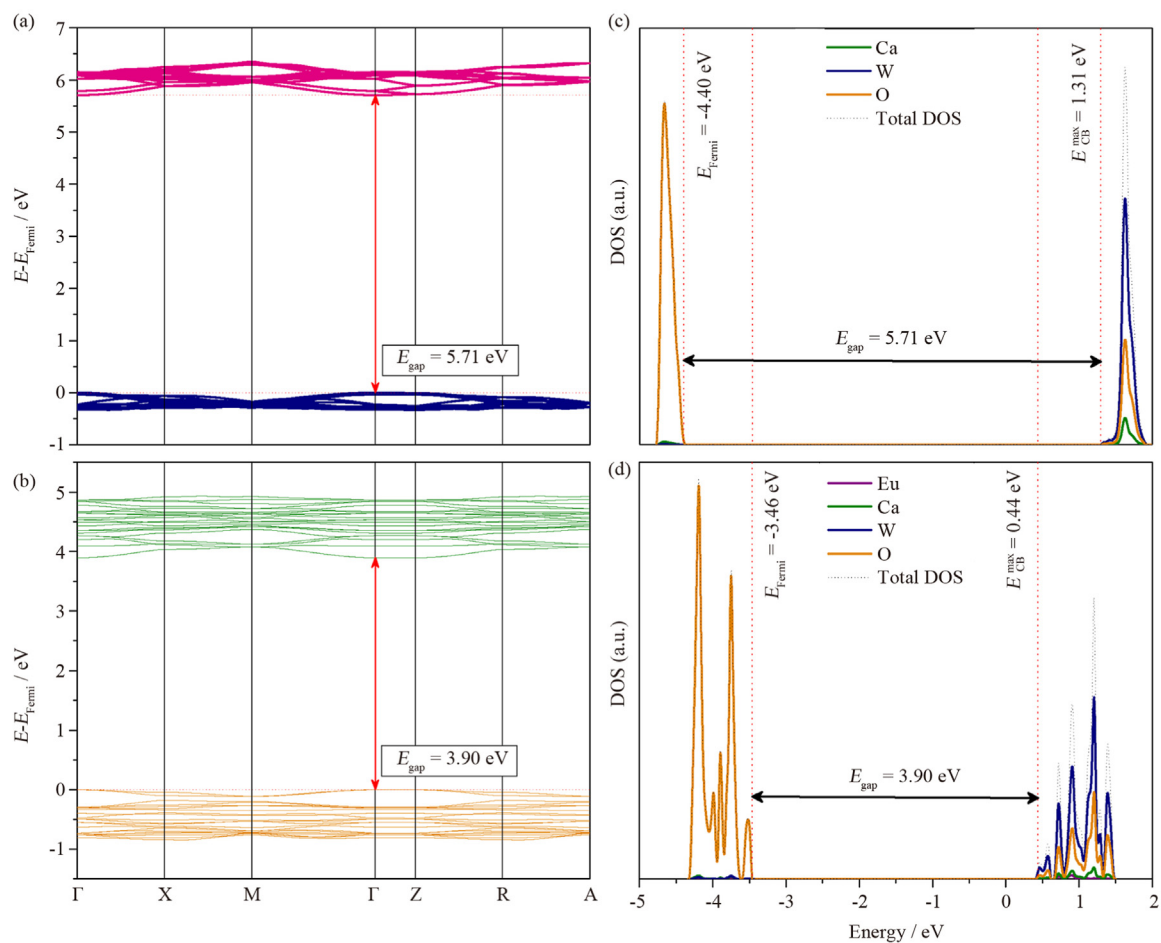


Fig. 4. Band structure for CW (a) and CWE (b) models and DOS for CW (c) and CWE (d) models.

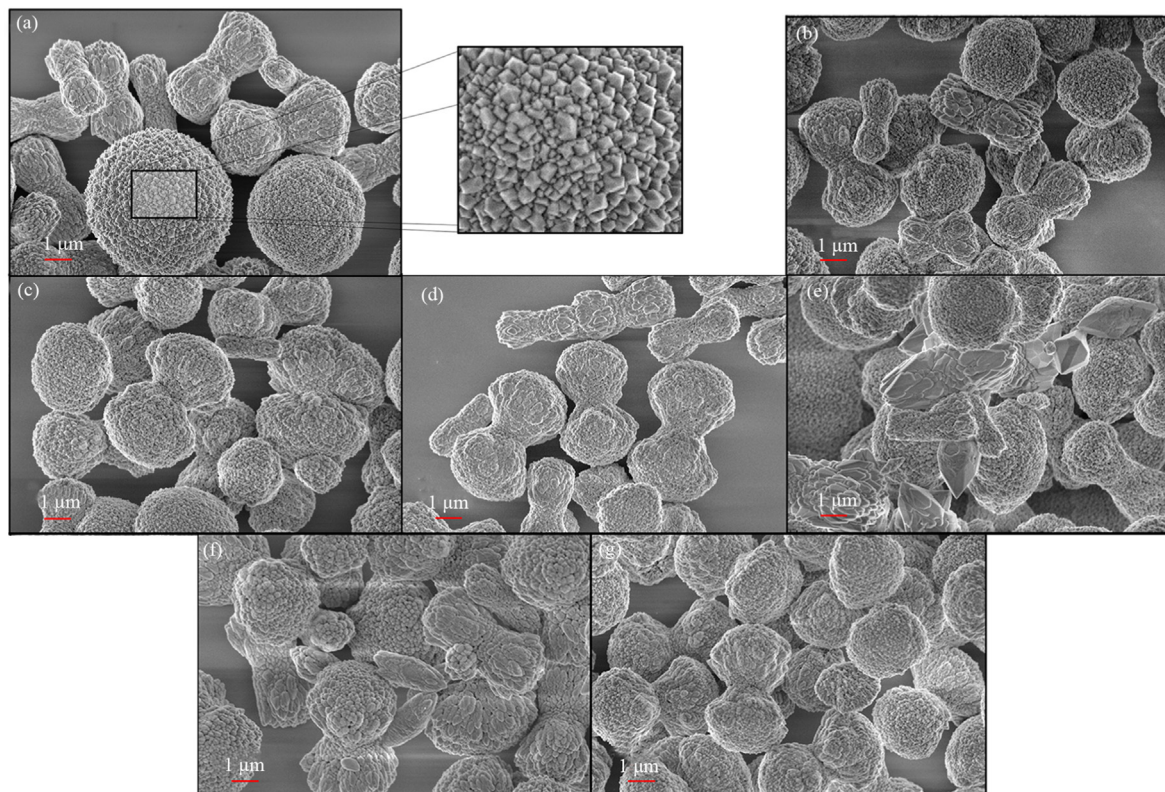


Fig. 5. FE-SEM images for the samples. (a) CW; (b) CWE1; (c) CWE2; (d) CWE4; (e) CWE6; (f) CWE8; (g) CWE10.

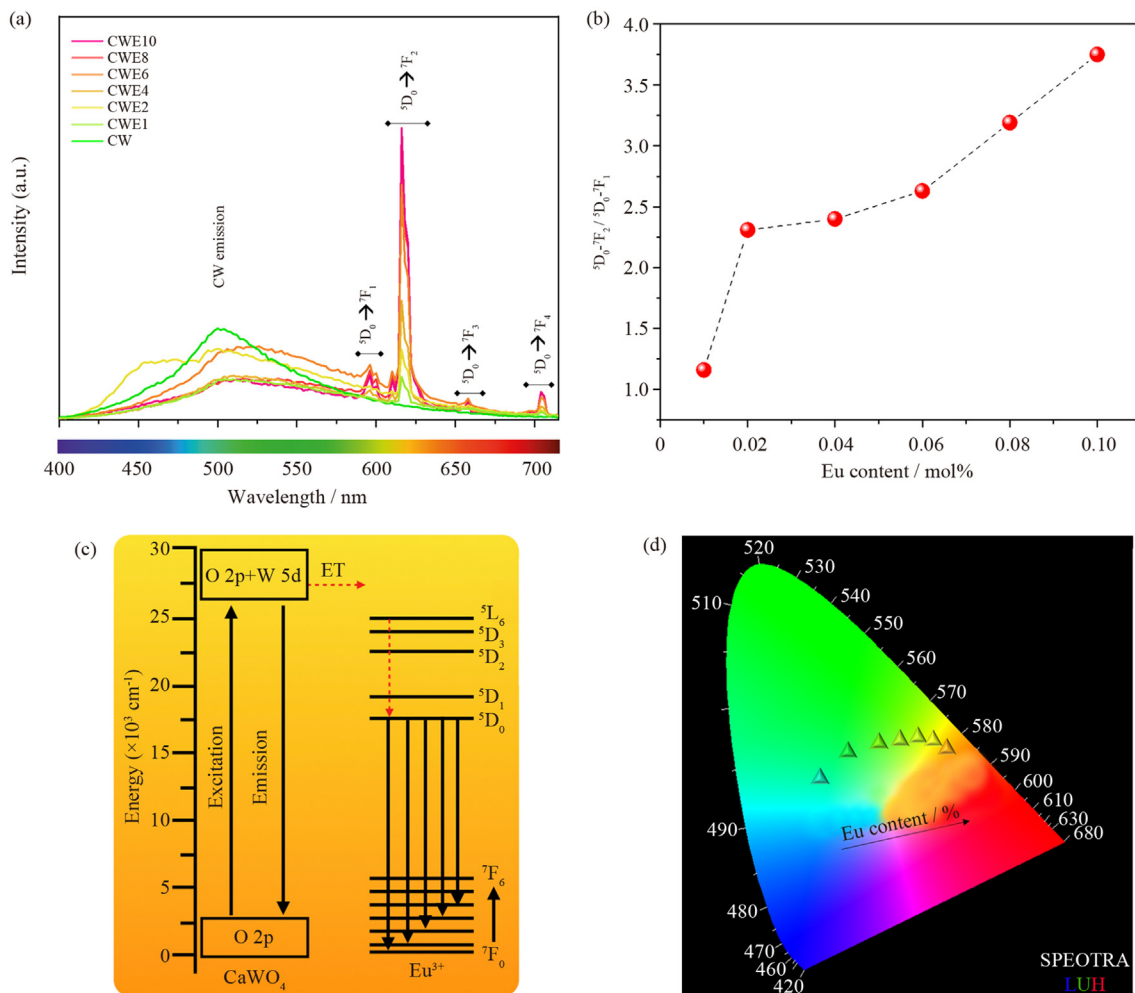


Fig. 6. (a) PL spectra for CW and CWE samples ($\lambda = 350$ nm); (b) Ratio of relative area for transitions ${}^5D_0 \rightarrow {}^7F_2 / {}^5D_0 \rightarrow {}^7F_1$; (c) Schematic luminescence model of CWE samples; (d) Coordinates of the Commission Internationale de l'Éclairage (CIE) by Spectralux software.

The peak located at 596 nm comes from a magnetic dipole transition ${}^5D_0 \rightarrow {}^7F_1$, that were almost independent of the local environment. The peak of greatest intensity, located at 616 nm, is called a hypersensitive red emission, and it comes from the transition of electric dipole ${}^5D_0 \rightarrow {}^7F_2$, that was strongly dependent on the environment. The appearance of this transition suggests that the Eu^{3+} cation is located in a symmetrical site where there is no inversion of symmetry,³⁹ while the absence of the transition ${}^5D_0 \rightarrow {}^7F_0$ implies that the Eu^{3+} cations are not occupying sites with C_s , C_n or C_{nv} symmetry.⁴⁰ The ratio of relative area of the ${}^5D_0 \rightarrow {}^7F_2$ to ${}^5D_0 \rightarrow {}^7F_1$ transitions provides information about the local distortions in the clusters which the Eu^{3+} cations were inserted into the structure.⁴¹ As presented in Fig. 6(b), when increasing the concentration of Eu^{3+} in the CWE samples, there is an increase in local distortions related to the $[\text{EuO}_8]$ clusters of the crystalline lattice.

Fig. 6(c) shows the schematic luminescence model of CWE samples. When the sample is excited, electrons are promoted from the VB, made up of the O 2p levels, to the CW CB, made up of the W 5d levels. The emission of these samples occurs when the excited electrons decay radiative from the CB to the VB, or when the electrons transfer from the CB to the excited levels of the Eu^{3+} cations. When populated, 4f states decay non-radiative to the level of emission characteristic of the Eu^{3+} cations (5D_0) and then

radiative to the fundamental states (7F_j , $j = 1, 2, 3$, and 4), emitting in the observed characteristic lengths.

The change in the color emission perceptible by the human eye of the CW and CWE samples was evaluated by the coordinates of the Commission Internationale de l'Éclairage (CIE) by Spectralux software⁴² from the emission spectra obtained under laser excitation at 350 nm (Fig. 6(d)). As expected, the CW has an emission in the cyan-green region, with a shift to orange with an increase in the substitution of Ca^{2+} by Eu^{3+} cations. This change occurs due to the sum of the characteristic emissions of Eu^{3+} cations in the red region (${}^5D_0 \rightarrow {}^7F_j$, $j = 1, 2, 3$, and 4) with the emissions of the CW matrix. Therefore, the ions substitution in a semiconductor matrix by Eu^{3+} cations can lead to modulation of the final characteristic emission, resulting in potential materials for application in optical devices.

The lifetimes of the CWE samples were calculated for the luminescence decay of ${}^5D_0 \rightarrow {}^7F_2$ transition, with emission and excitation fixed at 616 and 394 nm, respectively. Fig. SI-5 shows the mono exponential decay of the samples fitted with an exponential function as Eq. (4):

$$y = y_0 + A_1 \exp(t/\tau) \quad (4)$$

where, y is the intensity, y_0 the intensity at the 0 ms, A_1 the amplitude, and τ the lifetime of the transition ${}^5D_0 \rightarrow {}^7F_2$.

The τ values obtained for the CWE samples were close, being 0.70 ± 0.04 , 0.70 ± 0.04 , 0.72 ± 0.03 , 0.72 ± 0.02 , 0.70 ± 0.01 , and 0.67 ± 0.01 ms for samples CWE1, CWE2, CWE4, CWE6, CWE8, and CWE10, respectively. The CWE samples were fitted to a linear fit of $\lg y$ versus t , indicating that the samples have only one time of decay (see Fig. SI-5). These results indicate that Eu^{3+} cations occupy only one place of symmetry in the CW matrix and that there is only one process for the luminescence of the CWE samples.

4. Conclusions

In summary, the present work combines the experimental and theoretical results for better understanding of the PL emissions of the CW and CWE samples with different Eu^{3+} cations concentrations. First-principles calculations, within the framework of DFT, were performed to achieve a deeper understanding of the effects caused by the Eu^{3+} cations in the CW electronic structure in order to correlate with the PL emissions experimentally observed. These findings allow to find a luminescent material in which by varying the Eu^{3+} cations concentration, the color emissions can be modulated. This work also paves the way for the further design of CWE-based materials for various applications as red-blue phosphors in different kinds of display devices.

Acknowledgements

This work was funded in part by Fundação de Amparo à Pesquisa do Estado de São Paulo - FAPESP (2013/07296-2, 2016/23891-6, 2017/26105-4, 2019/01732-1), Financiadora de Estudos e Projetos - FINEP, Conselho Nacional de Desenvolvimento Científico e Tecnológico - CNPQ (166281/2017-4, 305792/2020-2), and CAPES. This work used computational resources of the "Centro Nacional de Processamento de Alto Desempenho em São Paulo" (CENAPAD-SP), "Centro de Computação John David Rogers" (CCJDR-UNICAMP), and the CENAPAD-RJ (SDumont). J.A. acknowledges Universitat Jaume I (project UJI-B2019-30), and the Ministerio de Ciencia, Innovación y Universidades (Spain) (project PGC2018094417-B-I00) for financially supporting this research. A.F.G acknowledges the Universitat Jaume I for the postdoctoral contract (POSDOC/2019/30).

Appendix A. Supplementary data

Supplementary data to this article can be found online at <https://doi.org/10.1016/j.jre.2021.08.023>.

References

- Yu MQ, Xu HY, Li YZ, Dai QL, Wang GF, Qin WP. Morphology luminescence and photovoltaic performance of lanthanide doped CaWO_4 nanocrystals. *J Colloid Interface Sci.* 2020;559:162.
- Chai RT, Liu YT, Zhang G, Feng JJ, Kang QW. *In situ* preparation and luminescence properties of CaWO_4 and $\text{CaWO}_4:\text{Ln}$ ($\text{Ln}=\text{Eu}^{3+}$, Tb^{3+}) nanoparticles and transparent $\text{CaWO}_4:\text{Ln}/\text{PMMA}$ nanocomposites. *J Lumin.* 2018;202:65.
- Bae Y-J, Lee KH, Byeon S-H. Synthesis and Eu^{3+} concentration-dependent photoluminescence of $\text{Gd}_{2-x}\text{Eu}_x\text{O}_3$ nanowires. *J Lumin.* 2009;129:81.
- Gracia L, Longo VM, Cavalcante LS, Beltran A, Avansi W, Li MS, et al. Presence of excited electronic state in CaWO_4 crystals provoked by a tetrahedral distortion: an experimental and theoretical investigation. *J Appl Phys.* 2011;110, 043501.
- Longo VM, Cavalcante LS, Paris EC, Sczancoski JC, Pizani PS, Li MS, et al. Hierarchical assembly of CaMoO_4 nano-octahedrons and their photoluminescence properties. *J Phys Chem C.* 2011;115:5207.
- Luo XF, Xie RJ. Recent progress on discovery of novel phosphors for solid state lighting. *J Rare Earths.* 2020;38:464.
- Bunzli JCG, Wang XJ, Chen XY. Preface to the special issue of rare earth luminescent materials. *J Rare Earths.* 2020;38:1.
- Bunzli JCG. On the design of highly luminescent lanthanide complexes. *Coord Chem Rev.* 2015;293:19.

- Zhu HM, Lin CC, Luo WQ, Shu ST, Liu ZG, Liu YS, et al. Highly efficient non-rare-earth red emitting phosphor for warm white light-emitting diodes. *Nat Commun.* 2014;5:4312.
- Carlos LD, Ferreira RAS, Bermudez VD, Ribeiro SJL. Lanthanide-containing light-emitting organic-inorganic hybrids: a bet on the future. *Adv Mater.* 2009;21:509.
- Richards BS. Luminescent layers for enhanced silicon solar cell performance: down-conversion. *Sol Energy Mater Sol Cells.* 2006;90:1189.
- Kang FW, Li LJ, Han J, Lei DY, Peng MY. Emission color tuning through manipulating the energy transfer from VO_4^{3-} to Eu^{3+} in single-phased $\text{LuVO}_4:\text{Eu}^{3+}$ phosphors. *J Mater Chem C.* 2017;5:390.
- Xie W, Mo YW, Zou CW, Kang FW, Sun GH. Broad color tuning and Eu^{3+} -related photo-emission enhancement via controllable energy transfer in the $\text{La}_2\text{Mg-GeO}_6:\text{Eu}^{3+},\text{Bi}^{3+}$ phosphor. *Inorg Chem Front.* 2018;5:1076.
- Zhang Y, Abraha A, Zhang R, Shahbazyan T, Fadavi M, Heydari E, et al. Luminescence properties of CaWO_4 and $\text{CaWO}_4:\text{Eu}^{3+}$ nanostructures prepared at low temperature. *Opt Mater.* 2018;84:115.
- Xiong S, Liang D, Wu H, Lin W, Chen JS, Zhang BS. Preparation, characterization, tribological and lubrication performances of Eu doped CaWO_4 nanoparticle as anti-wear additive in water-soluble fluid for steel strip during hot rolling. *Appl Surf Sci.* 2021;539:148090.
- Kaur P, Khanna A, Fabian M. Effects of annealing temperature on structural and photoluminescence properties of Eu, Dy and Sm doped CaWO_4 nanoparticles. *Ceram Int.* 2020;46:27262.
- Kaur P, Khanna A, Kaur J, Kumar R, Chandra R. Rare earth doped CaWO_4 and CaMoO_4 thin films for white light emission. *J Vac Sci Technol B.* 2021;39, 012205.
- Singh M, Ul Haq W, Bishnoi S, Singh BP, Arya S, Khosla A, et al. Investigating photoluminescence properties of Eu^{3+} doped CaWO_4 nanoparticles via Bi^{3+} amalgamation for w-LEDs application. *Mater Technol.* 2022;37:1051.
- Oliveira MC, Ribeiro RAP, Gracia L, Lazaro SR, Assis M, Oliva M, et al. Experimental and theoretical study of the energetic, morphological, and photoluminescence properties of $\text{CaZrO}_3:\text{Eu}^{3+}$. *CrystEngComm.* 2018;20:5519.
- Goncalves RF, Cavalcante LS, Nogueira IC, Longo E, Godinho MJ, Sczancoski JC, et al. Rietveld refinement, cluster modelling, growth mechanism and photoluminescence properties of $\text{CaWO}_4:\text{Eu}^{3+}$ microcrystals. *CrystEngComm.* 2015;17:1654.
- Dovesi R, Erba A, Orlando R, Zicovich-Wilson CM, Civalleri B, Maschio L, et al. *Quantum-mechanical condensed matter simulations with CRYSTAL*. vol. 8. Wiley Interdisciplinary Reviews-Computational Molecular Science; 2018:1.
- Dovesi R, Saunders VR, Roetti C, Orlando R, Zicovich-Wilson CM, Pascale F, et al. *CRYSTAL17 user's manual*. Torino: University of Torino; 2017.
- Becke AD. Density-functional thermochemistry. 3. The role of exact exchange. *J Chem Phys.* 1993;98:5648.
- Lee CT, Yang WT, Parr RG. Development of the Colle-Salvetti Correlation-energy formula into a functional of the electron-density. *Phys Rev B Condens Matter.* 1988;37:785.
- Dovesi R, Orlando R, Civalleri B, Roetti C, Saunders VR, Zicovich-Wilson CM. Crystal basis sets library. <http://www.crystal.unito.it/basis-sets.php>.
- Crystal. Basis sets library. http://www.crystal.unito.it/Basis_Sets/Ptable.html.
- Gomez GE, Lopez CA, Ayscue RL, Knope KE, Deluigi MDT, Narda GE. Strong photoluminescence and sensing performance of nanosized $\text{Ca}_{(0.8)}\text{Ln}_{(0.1)}\text{Na}_{(0.1)}\text{WO}_4$ ($\text{Ln} = \text{Sm}, \text{Eu}$) compounds obtained by the dry "top-down" grinding method. *Dalton Trans.* 2019;48:12080.
- Klug HP, Alexander LE. *X-ray diffraction procedures: for polycrystalline and amorphous materials*. 2nd ed. Wiley-VCH; 1974.
- Jayachandriah C, Kumar KS, Krishnaiah G, Rao NM. Influence of Dy dopant on structural and photoluminescence of Dy-doped ZnO nanoparticles. *J Alloys Compd.* 2015;623:248.
- Tiseanu C, Cojocaru B, Parvulescu VI, Sanchez-Dominguez M, Primus PA, Boutonnet M. Order and disorder effects in nano-ZrO₂ investigated by micro-Raman and spectrally and temporally resolved photoluminescence. *Phys Chem Chem Phys.* 2012;14:12970.
- Ningombam GS, Nongmaithem RS. Morphology and photoluminescence of self-assembled $\text{CaWO}_4:\text{Sm}^{3+}$ microspheres: effect of pH and surfactant concentration. *Int Nano Lett.* 2017;7:133.
- Chen GQ, Wang FL, Ji WC, Liu YX, Zhang X. Improved luminescence of $\text{CaWO}_4:\text{Eu}^{3+}$ microspheres by codoping Gd^{3+} . *Superlattice Microsc.* 2016;90:30.
- Janbu J, Mayamae J, Wirunchit S, Baitahe R, Vittayakorn N. Directed synthesis, growth process and optical properties of monodispersed CaWO_4 microspheres via a sonochemical route. *RSC Adv.* 2015;5:19893.
- Ningombam GS, Singh NR, Ningthoujam RS. Controlled synthesis of $\text{CaWO}_4:\text{Sm}^{3+}$ microsphere particles by a reverse-micelle method and their energy transfer rate in luminescence. *Colloid Surface Physicochem Eng Aspect.* 2017;518:249.
- Goncalves RF, Godinho MJ, Marques APA, Santos MRC, Rosa ILV, Longo E, et al. Structure, morphology, and optical properties of $(\text{Ca}_{(1-3x)}\text{Eu}_{(2x)})\text{WO}_4$ microcrystals. *Electron Mater Lett.* 2015;11:193.
- Cavalcante LS, Longo VM, Sczancoski JC, Almeida MAP, Batista AA, Varela JA, et al. Electronic structure, growth mechanism and photoluminescence of CaWO_4 crystals. *CrystEngComm.* 2012;14:853.
- Mazzo TM, Pinatti IM, Macario LR, Avansi W, Moreira ML, Rosa ILV, et al. Europium-doped calcium titanate: optical and structural evaluations. *J Alloys Compd.* 2014;585:154.

38. Wang WX, Yang PP, Gai SL, Niu N, He F, Lin J. Fabrication and luminescent properties of $\text{CaWO}_4:\text{Ln}^{3+}$ (Ln = Eu, Sm, Dy) nanocrystals. *J Nanopart Res.* 2010;12:2295.
39. Pinatti IM, Nogueira IC, Pereira WS, Pereira PFS, Gonçalves RF, Varela JA, et al. Structural and photoluminescence properties of Eu^{3+} doped $\alpha\text{-Ag}_2\text{WO}_4$ synthesized by the green coprecipitation methodology. *Dalton Trans.* 2015;44:17673.
40. Su YG, Li LP, Li GS. Synthesis and optimum luminescence of CaWO_4 -based red phosphors with codoping of Eu^{3+} and Na^+ . *Chem Mater.* 2008;20:6060.
41. Volanti DP, Rosa ILV, Paris EC, Paskocimas CA, Pizani PS, Varela JA, et al. The role of the Eu^{3+} ions in structure and photoluminescence properties of $\text{SrBi}_2\text{Nb}_2\text{O}_9$ powders. *Opt Mater.* 2009;31:995.
42. Stearns EI. *Commission Internationale de L'Éclairage, Colorimetry. Color Res. Appl.* 2nd ed. vol. 13. Gaithersburg, MD: Central Bureau of the CIE; 1987. Publication CIE No. 15.2, 78; Central Bureau of the CIE.